AFAPL-TR-78-62

LEVEL

VIBRATORY RESPONSE OF A ROTATING DISK INCORPORATING IMAGE DEROTATION TECHNIQUES AND HOLOGRAPHIC INTERFEROMETRY

Propulsion Branch
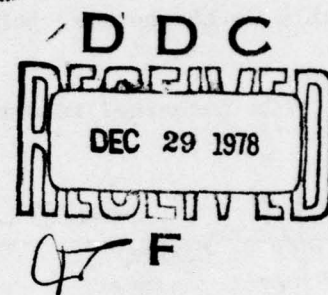Turbine Engine Division

John E. Horner
James C. MacBain
William A. Stange

DDC
RECEIVED
DEC 29 1978
F

September 1978

TECHNICAL REPORT AFAPL-TR-78-62

Final Report for Period June 1977 to December 1977

Approved for public release; distribution unlimited.

AIR FORCE AERO-PROPULSION LABORATORY
AIR FORCE WRIGHT AERONAUTICAL LABORATORIES
AIR FORCE SYSTEMS COMMAND
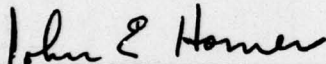WRIGHT-PATTERSON AIR FORCE BASE, OHIO 45433
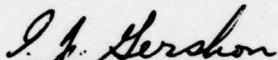
ADA062671

78 12 28 003

NOTICE

When Government drawings, specifications, or other data are used for any purpose other than in connection with a definitely related Government procurement operation, the United States Government thereby incurs no responsibility nor any obligation whatsoever; and the fact that the government may have formulated, furnished, or in any way supplied the said drawings, specifications, or other data, is not to be regarded by implication or otherwise as in any manner licensing the holder or any other person or corporation, or conveying any rights or permission to manufacture, use, or sell any patented invention that may in any way be related thereto.
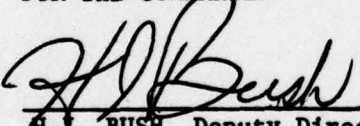
This report has been reviewed by the Information Office (OI) and is releasable to the National Technical Information Service (NTIS). At NTIS, it will be available to the general public, including foreign nations.

This technical report has been reviewed and is approved for publication.

JOHN E. HORNER
Project Engineer
Propulsion Branch

I.J. GERSON, Tech Area Manager
Propulsion Branch
Turbine Engine Division

FOR THE COMMANDER

H.I. BUSH, Deputy Director
Turbine Engine Division
Air Force Aero-Propulsion Laboratory

"If your address has changed, if you wish to be removed from our mailing list, or if the addressee is no longer employed by your organization please notify AFAPL/TFA____,W-PAFB, OH 45433 *to help us maintain a current mailing list".*

Copies of this report should not be returned unless return is required by security considerations, contractual obligations, or notice on a specific document.

62203 F

REPORT DOCUMENTATION PAGE		READ INSTRUCTIONS BEFORE COMPLETING FORM
1. REPORT NUMBER AFAPL-TR-78-62	2. GOVT ACCESSION NO.	3. RECIPIENT'S CATALOG NUMBER
4. TITLE *(and Subtitle)* VIBRATORY RESPONSE OF A ROTATING DISK INCORPORATING IMAGE DEROTATION TECHNIQUES AND HOLOGRAPHIC INTERFEROMETRY		5. TYPE OF REPORT & PERIOD COVERED FINAL REPORT. 1 Jun 1977 — 1 Dec 1977
		6. PERFORMING ORG. REPORT NUMBER
7. AUTHOR(s) John E. Horner James C. MacBain William A. Strange		8. CONTRACT OR GRANT NUMBER(s)
9. PERFORMING ORGANIZATION NAME AND ADDRESS Air Force Aero-Propulsion Laboratory/TBP Wright-Patterson AFB, Ohio 45433		10. PROGRAM ELEMENT, PROJECT, TASK AREA & WORK UNIT NUMBERS 646100 306612 3066 30661221
11. CONTROLLING OFFICE NAME AND ADDRESS Air Force Aero-Propulsion Laboratory/TBP Wright-Patterson AFB, Ohio 45433		12. REPORT DATE September 1978
		13. NUMBER OF PAGES 64
14. MONITORING AGENCY NAME & ADDRESS*(if different from Controlling Office)* 62 p.		15. SECURITY CLASS. *(of this report)* UNCLASSIFIED
		15a. DECLASSIFICATION/DOWNGRADING SCHEDULE

16. DISTRIBUTION STATEMENT *(of this Report)*

Approved for public release; distribution unlimited.

17. DISTRIBUTION STATEMENT *(of the abstract entered in Block 20, if different from Report)*

18. SUPPLEMENTARY NOTES

19. KEY WORDS *(Continue on reverse side if necessary and identify by block number)*

Rotating Disk	Holography
Image Derotation	Vibration
Finite Element Analysis	

20. ABSTRACT *(Continue on reverse side if necessary and identify by block number)*

This report covers work carried out at AFAPL's Turbo Structures Research Laboratory (TSRL) on the vibratory response of an internally clamped annular disk under both static and rotational conditions. Standard holographic interferometry was used to experimentally determine the frequencies and mode shapes of a 10 inch disk under nonrotating conditions. Incorporating an image derotator and double-pulsed ruby laser, resonant conditions and mode shapes were again determined, but this time the interferograms were constructed while the disk was rotating at specified speeds. The finite element computer program NASTRAN was

DD FORM 1473 EDITION OF 1 NOV 65 IS OBSOLETE
1 JAN 73

011570

78 12 28 003

used to model the steel disk and analytically determine the mode shapes and frequencies as a function of speed. The analytical frequency predictions were compared to the experimental results and found to deviate by about 4%.

FOREWORD

A combined numerical-experimental study was performed in the Turbo-Structures Research Lab (TSRL) between 1 June 1977 and 1 December 1977. The purpose was to investigate the vibratory response of an internally clamped annular disk under both static and rotational conditions.

A 10 inch diameter steel disk with an integral hub was manufactured. Holographic interferometry was used to experimentally determine the frequencies and mode shapes for the first five diametrical modes and one complex mode under nonrotating conditions. Incorporating an image derotator and a double-pulsed ruby laser, resonant conditions and mode shapes were again determined for the above modes, but this time the interferograms were constructed while the disk was rotating at specified speeds.

The finite element computer program NASTRAN was used to model the steel disk and analytically determine the mode shapes and frequencies. For the nonrotating case, all mode shapes and frequencies were determined and compared to the corresponding modes found experimentally. Under conditions of rotation, only the third diametrical mode was studied as a function of centrifugal loading because of the large requirement for computer central memory and associated expense. The resulting frequency predictions were compared to the experimental findings with a deviation of about 4%.

TABLE OF CONTENTS

LIST OF ILLUSTRATIONS

LIST OF ILLUSTRATIONS (CONTINUED)

LIST OF TABLES

NOMENCLATURE

n	Nodal Diameter
s	Nodal Circle
W	Out-of-Plane Displacement
P	Excitation Force
F_E	Excitation Frequency
t	Time
A	Resonant Amplitude
θ_o	Absolute Angular Coordinate of Disk
P_n	Disk Vibration Frequency
Ω	Angular Velocity of Disk
θ	Angular Coordinate of Disk
a	Disk Outer Radius
b	Disk Inner Radius
T	Thickness
λ^2	Eigenvalue
ω	Frequency
ρ	Mass/Area
E	Young's Modulus
ν	Poisson's Ratio
D	Flexural Rigidity
δ	Density
σ_a	Average Stress
Ω_c	Critical Speed

SECTION I

INTRODUCTION

Rotating disk-like structures are encountered throughout the engineering development of advanced gas turbine engines and have been the object of study since the appearance of the steam turbine (Reference 1). They possess several families of modes of free vibration comprised of both circumferential and diametral modes, each having an infinite number of possible resonant frequencies. Each resonant response corresponds to a deflection pattern comprised of nodal lines which can rotate relative to the disk or remain fixed to the disk depending on the relative phase shifts as the structure passes through resonance. These responses are difficult to characterize because the maximum stress or strain location is constantly changing for each mode of vibration in a particular family.

Resonant frequencies of the disk are affected by the various operating conditions such as rotational speed, temperature, pressure, and boundary effects. Fatigue damage can accumulate quite rapidly when the structure operates within a resonant band, especially when it does not possess sufficient damping or when it passes too slowly through this condition. The excitation forces which can excite resonance in a rotating disk are numerous. Dynamic unbalance, oil pumps, gear meshing, ball bearings, engine struts, pressure differentials, and a variety of other sources may excite a disk at frequencies from fractional to multiple orders of engine speed. They can excite disk-like structures into large deflections where nonlinearities can occur. Under dynamic conditions, the nonlinear systems may respond to frequencies equal to and/or in multiples of the forcing frequency. Their occurrences are accompanied by fatigue damage accumulating at a rate higher than expected, and at a resonance which may occur at frequencies removed from the forcing frequencies.

Analytically, it is difficult if not impossible to currently predict the structural response of disk-like structures operating within a turbine engine environment. In order to establish and verify the vibrational characteristics of these structures, they must be manufactured and tested experimentally. This is usually accomplished by instrumenting with strain gages and recording the output via telemetry or slip rings. This method suffers from mechanical/electrical linkage problems and, perhaps more often, from inadequate placement of the gages themselves. Data reduction and interpretation of results are difficult and cumbersome.

Through the advent of holography, alternative methods have been established to determine the response of structures as a function of various forcing frequencies under nonrotating conditions. Mode shapes and frequencies are readily determined for the full surface of the structure, a feature which often leads to quick identification of areas of high stress concentrations. However, effects of changing boundary conditions on structural stiffness, and the resulting resonant conditions as a function of centrifugal loading could not be investigated because of the rigid requirements of no relative movement required to conduct holographic interferometry.

As early as 1970 (Reference 2), researchers have attempted to apply holographic interferometry to rotating objects. Success was met through an Air Force contract granted to United Technologies Research Center in developing an optical system for dynamic analysis of rotating structures (Reference 3). The method uses an image derotator to optically compensate or stop the motion of the object, giving it the appearance of a stationary object. It gives continuous motion compensation of the object and allows double pulse holography to be performed while the object is rotating and viewed through the image derotator. Once the holographic film is developed, the out-of-plane displacement and resulting mode shapes can be photographed and studied when the film is illuminated by a laser light. The system was delivered to the Air Force and installed in the Turbo-Structures Research

Lab (TSRL). The present work was to install the system, experimentally determine the resonant mode shapes and frequencies for a rotating disk, and verify these results through the utilization of numerical techniques. Discussed will be the theoretical aspects of disk vibration, mode shape determinations under nonrotating conditions, the same modes as a function of increasing speed or centrifugal loading and the results of the finite element program NASTRAN used to verify the experimental results.

SECTION II

DISCUSSION

1. DISK VIBRATION

Assume a circular disk fixed at its center and unconstrained along its outer periphery. The modes of vibration may be composed of nodal diameters (n), nodal circles (s), or combinations of nodal diameters and circles (Reference 4). Discussion shall concern those modes containing only nodal diameters, though arguments are equally applicable to a combination of nodal diameters and circles. Modes comprised of nodal circles shall not be addressed in this discussion. They require axisymmetric forcing functions to drive them which are rarely encountered in practice.

The vibration of the nonrotating disk vibrating in the nth nodal diameter excited by a stationary force varying sinusoidally in time, $P\cos F_E t$, can be described by:

$$W = A \sin n\,\theta_0 \cos p_n t \tag{1}$$

where W is the transverse displacement, and $A \sin n\,\theta_0$ indicates the shape of vibration; A is the resonant amplitude, which is a function of the disk radius and proportional to the magnitude of the excitation force, P. The absolute angular coordinate of the disk relative to inertial space is denoted by θ_0. (See Figure 1 for clarification of notation.) Likewise, $\cos p_n t$ is the harmonic movement, with p_n being the vibration frequency and t the time. Resonance will occur when the excitation frequency, F_E, is equal to p_n.

We can use a trigonometric identity to put Equation 1 in the form:

$$W = \frac{A}{2} \sin (n\,\theta_0 - p_n t) + \frac{A}{2} \sin (n\,\theta_0 + p_n t) \tag{2}$$

which can be considered as the superposition of two traveling waves of shape $\frac{A}{2} \sin n\theta_0$. Now, if the disk is rotated at an angular velocity, Ω, the absolute angular coordinate, θ_0, is related to the angular position of the disk, θ, by $\theta_0 = \theta - \Omega t$. Substituting, Equation 2 becomes:

$$W = \frac{A}{2} \sin [n\theta - (p_n + n\Omega) t] + \frac{A}{2} \sin [n\theta + (p_n - n\Omega) t] \qquad (3)$$

Looking at Equation 3, we see that, under conditions of rotation, the disk resonance will occur when the excitation frequency, F_E, is such that $F_E = p_n \pm n\Omega$. This is saying that two excitation frequencies will excite the same resonant mode at a given rpm. For example, the 2n mode of vibration will be excited into resonance by two different excitation frequencies, one that is 2Ω greater than the 2n natural frequency and one that is 2Ω less than the 2n natural frequency. A typical frequency speed diagram demonstrating this phenomena is shown in Figure 1.

Here, line AB represents the natural frequency of the disk for the nth mode of vibration as a function of speed, Ω. The increase in frequency is attributed to the centrifugal stiffening as a result of rotation. Lines AC and AD represent the upper and lower resonant conditions, $F_{E2} = P_n + n\Omega_0$ and $F_{E1} = p_n - n\Omega_0$ respectively. Thus, at speed Ω_0 resonance will exist as indicated by the applied frequencies F_{E2} and F_{E1}. Experimentally, line AB is easily established by bisecting the upper and lower curves of AC and AD which are determined by monitoring disk transverse displacement for increasing values of rpm. This line, which depicts the natural frequency of the disk, was later verified for the 3n mode by utilizing finite element techniques. At point D, when $n\Omega_c = p_n$, an interesting phenomenon occurs. Here the speed of rotation equals Ω_c and

resonance can result from a stationary force P, which has an excitation
frequency, F_E, equal to zero. (This is equivalent to a stationary force
P traveling at $n\Omega$ around the rim of a stationary disk.) In a turbine
engine, this condition can occur quite readily within the speed range of
a given compressor stage. Attempts to operate in this region for pro-
longed periods of time are therefore avoided. For speeds in excess of
Ω_c, two more resonant frequencies are found for each value of speed.
Line DE is the mirror image of the extension of AD and represents the
case when $P_n = - (F_E - n\Omega)$, which provides a positive value for p_n when
$F_E < n\Omega$.

2.   EXPERIMENTAL PROCEDURES - STATIC CONDITIONS

A circular disk was manufactured from 1018 cold-rolled steel. It
had a constant thickness of 0.0625 inches, with an outside diameter of
10 inches. Integrally formed with the disk was a center hub which was
1.0 inch in diameter and 1.0 inch thick, and had a center bore hole of
0.5 inches for sliding onto the shaft of a drive spindle. The transition
from the hub to the disk was made with a 1/16 inch radius fillet.

Initially, the disk was statically mounted to an isolation table
and its first five diametral modes of vibration (1n, 0s) through (5n, 0s)
and the second coupled mode of vibration (2n, 1s) determined using time
average holography. In classifying the different modes of vibration, n
refers to the number of nodal diameters and s refers to the number of
nodal circles, not including the inner fixed boundary.

Under static conditions, holography is an ideal method of experi-
mentally determining the natural modes and frequencies. As early as
1965 (Reference 5), holographic interferometry was first used to study
vibrating objects. It has since proved useful throughout the aerospace

industry for vibration analysis of critical components such as compressor blades and disks. Unlike strain gages and photoelastic coatings, holography is a non-intrusive optical technique that does not affect the mode shapes or response of the structure. The object can be of any shape with the final results being a full field picture of the vibrating displacement of the object. A simple explanation of the technique follows:

A hologram, which is a photograph containing information about intensity and phase of light reflected by an object, is made when a high resolution photographic plate is exposed to two beams of coherent light waves intersecting at the surface of the photographic plate. One of the beams is classified as the reference beam and comes unobstructed from the laser. The other beam, known as the object beam, comes from the laser but is first reflected off an object before reaching the photographic plate. The fact that the light waves are coherent (light waves traveling through space are of the same frequency and phase) enables a grating to be formed on the plate. This grating is formed from the constructive and destructive interference of the two light beams, i.e., object beam and reference beam. After the exposed plate has been developed, returned to its original position, and illuminated by a coherent beam, the grating on the plate will cause the light to be bent or diffracted such that the object beam is recreated. This beam, which was originally diffracted off the object, reconstructs the image of the object appearing in its original position in space, provided all of the factors are the same as in the original exposure. In order to view the reconstructed image, one looks through the hologram and sees the image appearing in space. This is known as transmission holography.

In using the technique for vibration analysis, a transmission hologram is made of the object to be analyzed (a disk in this case) while it is stationary. The hologram is developed and placed in its original position and one observes, while looking through the plate, the original object and, superimposed on it, the image of the object reconstructed by

the hologram. If the object is vibrating, the resulting displacement
will cause fringes to appear. These are caused by the light rays from
the object interfering with those from the image, and correspond to the
displacement of the object from its original stationary position. When
the object undergoes a sinusoidal forced vibration, fringes will be seen
on the object only when all points on the object are vibrating in phase
or 180° out of phase with each other. Such is the case when an elastic
body is vibrating at one of its natural frequencies. Thus, by sweeping
through the frequency range of interest, the natural frequencies and mode
shapes can be determined by observing the frequencies at which fringes
occur and how they are distributed. This type of testing is termed "real-
time" holography, in that the fringes appear or disappear as a result of
the sinusoidal forced vibration.

Once the natural frequencies of the object are determined using
"real-time" holography, permanent photographs of the mode shapes can be
recorded using time-averaged holography. This method consists of expos-
ing the holographic plate with reflected coherent light from the object
while it is vibrating at one of its natural frequencies. The resulting
hologram, after proper development, shows the object to be covered with
interference fringes. These fringes are caused by interference when the
object is at its two extreme oscillatory excursions. The points on the
object which have no relative motion, i.e., the nodal lines, reflect the
most light and appear as the brightest fringes in the hologram. As we
travel outward from the nodal lines, each fringe encountered represents
a contour of constant displacement. Hence, the time-averaged hologram
yields a contour map of the normal displacement. This can be easily pho-
tographed by using common high contrast photographic films.

The experimental set-up used to determine the natural modes and
frequencies of the steel disk are shown in Figures 2 and 3. A HeNe 50
MW laser (Spectra Physics 125A) was used as a light source. As shown in
Figure 3, the laser beam is reflected off mirrors (M) and is divided into
two parts by the beam splitter (BS). The object beam (O) is expanded by

the beam expander (BE). The beam then passes to another beam splitter which reflects the light to the disk. The purpose of this beam splitter is to make the light waves perpendicular to the disk so that optimum illumination, especially under rotating conditions, will be achieved by using retro-reflective paint applied to the surface of the disk. The object beam is then reflected from the disk and onto the photographic plate (Agfa - Gevaert 10E75). Finally, the reference beam (R) via the beam splitter, mirrors, and expanders goes directly to the photographic plate. The interference of the two beams at the photographic plate enables a hologram (real-time or time-averaged) to be made of the circular disk.

3.   EXPERIMENTAL PROCEDURES - ROTATING CONDITIONS

After determining the mode shapes and frequencies under static conditions, the disk was mounted to a 3/4 HP tool post-grinder with a speed capability ranging from zero to 10,000 rpm. The first five diametral modes of vibration (1n, 0s) through (5n, 0s) and the second couple mode of vibration (2n, 1s) were determined using image derotated double-pulsed holography as a function of speed. This method incorporates an image derotator, developed by P. Waddell (Reference 6), to compensate optically for the circular motion of the object giving it the appearance of a stationary object. Stetson (Reference 3) applied the image derotator in conjunction with standard double-pulsed laser holography and demonstrated that interferometric holograms could be recorded of objects rotating at high speeds. (This work was funded by the Air Force Aero-Propulsion Laboratory under Contract F33615-75-C-2013.) The work culminated in the delivery and installation of an image derotator system at Wright-Patterson Air Force Base. It was this instrument which was used to record the vibration characteristics of the spinning disk. An important advantage of this system over stroboscopic methods for stopping the rotation of an object is its ability to provide continuous motion compensation of the object. This is independent of the size of the object and is limited only by the mechanics of rotating the prism, so that tolerances on laser pulse width and pulse repetition rate are greatly relaxed.

9

As mentioned previously, a double-pulsed ruby laser (Apollo Model 22HD) was used in conjunction with the image derotator to obtain holograms under conditions of rotation. The fringes formed represent contours of constant vibratory displacement. It should be mentioned that P. Waddell (Reference 2) has made attempts to use a brute force method of gating a laser into one pulse per revolution so that holographic interferometry could be accomplished without an image derotator. Extreme difficulty is encountered in maintaining registration of the hologram and object (i.e., shaft whirl). This together with the low laser energy inherent to the short pulses required to stop the rotary motion, make this method extremely unattractive. However, by incorporating an image derotator, the object appears stationary and the problems of maintaining registration of the holograms over a cycle of revolution and the problems associated with gating the laser are eliminated.

The experimental set-up used to determine the mode shapes and frequencies under rotating conditions is shown in Figure 4. This is a standard off-axis holographic set-up. A Q-switched pulsed ruby laser is used for generating the laser light. It passes through a beam expander and onto a beam splitter. The light that is transmitted becomes the object beam, reflecting through a large double folding mirror assembly (M1) which directs it to the disk. By virtue of retro-reflective paint on the disk, the beam is reflected back and retraces the same path back to the beam splitter (BS) where it is directed through the derotator onto the holographic film. The reflected light from the beam splitter acts as the reference beam. It is reflected off mirror M2 onto mirror M3 and then onto the holographic film.

The image derotator shown in Figure 5, which is the most complex portion of the holographic set-up, is comprised of a transmissive folded Abbe prism (Supplied by Optical Systems and Technology, Inc., East Hartford, Connecticut) which is located within a hollow shaft motor comprised of an air bearing and a brushless DC torque motor. A code wheel that has a number of equally spaced circumferential markers is attached to the

derotator shaft. A light-emitting diode (LED) is used to detect the markers on the code wheel and thus monitor the rotational speed and phase of the motor. Another code wheel shown in Figure 6 is fixed to the shaft of the lathe motor which drives the disk. It also has a LED pickup. The signal which is received from this pickup is compared to the derotator signal via a control box unit. This unit adjusts the voltage to the derotator motor so that its rotational rate is half that of the rotating disk and is phase-locked with it. Also shown is an electromagnet used to excite the disk and a capacitance pickup used to detect resonance.

Because the derotator is traveling at half the angular velocity of the object, continuous motion compensation is achieved. An explanation of the principles involved follows. Figure 7 is a diagram of a folded Abbe prism, which is comprised of three prisms mated together, and is located in the center of the derotator. Note, the top and bottom surfaces of the prism system are mirrored and thus reflect the light waves. Also, depending on the relative angle in which the light waves strike the interfacing surfaces of the prisms, the light is either reflected or transmitted. Now, if an object (note arrow in vertical position) is viewed through the wedged prism system, it appears to be inverted. Rotate the object 180° in the clockwise direction and the derotator 90° in the same direction, remembering the derotator travels at half the speed of the object, the object as viewed through the prism remains stationary. Again, rotate the object another 180° and correspondingly the derotator 90°. Observe the arrowhead remains in the same position. Therefore, for any angular position of the object, it appears stationary as viewed through the derotator prism system, provided the prism system is rotated at half the angular speed of the object. This is the principle on which the derotator works. A more thorough explanation of the system is found in Reference 3.

The disk shown in Figures 7 and 8 was driven by means of a 3/4 HP tool post-grinder motor connected by a belt to a two-bearing internal grinding spindle. The disk was machined with a 0.50 inch diameter hole for sliding onto a half-inch drive spindle. A keyway was used to prevent slippage of the disk relative to the spindle. A 3/8 inch-16 nut applied with a torque of 100 inch-lb fixed the disk to the spindle. Fixed to the opposite end of the spindle was the code wheel. This drive system had a capability of 10,000 rpm which is the upper limitation of the derotator. Prior to spinning the disk, its burst speed was calculated to ensure operator safety. The results (see Appendix A) indicates a safety margin of approximately two which was considered sufficient. The drive system was more than adequate to achieve a true center of rotation of the disk, a requirement necessary to provide continuous alignment between the disk axis of rotation and the derotator optical axis of rotation. The rotational speed of the grinder was controlled by a simple rheostat.

To excite the disk under conditions of rotation into one of its resonant modes, either an electromagnet or siren was used. It was placed a fixed distance parallel to the disk surface at its outer circumference and driven by a sweep oscillator. A stationary vibration pickup, typically a capacitance probe, was placed near the back face of the disk to monitor out-of-plane displacement. As in the nonrotating configuration, the excitation frequency signal and the frequency signal from the capacitance pickup were fed respectively to the horizontal and vertical plates of an oscilloscope. The resulting Lissajous patterns were used to determine resonance. Figure 9 shows the instrumentation used to establish this condition. Holographic interferograms using the derotator in conjunction with the ruby laser were made at various resonant conditions as a function of speed. The excitation frequency and disk rpm were recorded for each of these interferograms. In this manner, a frequency-speed diagram showing the various resonant conditions for the spinning disk was generated.

Two factors should be noted in utilizing the image derotator for execution of holographic interferometry as described above. First, the reference beam does not pass through the derotator and hence remains linearly polarized throughout its path of travel. The object beam by virtue of passing through the derotator undergoes a change in polarization. To record a hologram, this light must have the same polarization as the intended reference beam. Fortunately, as noted by Stetson (Reference 3), the construction of the folded Abbe inverting prism afforded the characteristics of a half-wave retarding plate. By simply placing a quarter-wave retarder plate at the derotator entrance, the reflected linearly polarized object beam is converted to circular polarized light. The beam is converted back to linearly polarized light with another quarter-wave retarder after the derotator. Thus, it is possible to achieve nearly complete polarization compensation.

Secondly, since the object is illuminated with linearly polarized light, under conditions of rotation, the reflected light will undergo a cyclic change in orientation relative to the derotated image of the disk. In other words, the image appears stationary but the linearly polarized light is rotating at the angular velocity of the disk and in the opposite direction. There would be a total lack of correlation and hence no interferogram if the disk were allowed to rotate more than 90° between pulses of the ruby laser. This was easily accomplished by limiting the laser pulse width to less than 50 μs. At 10,000 rpm, this would amount to less than 3° of disk rotation.

4.   ALIGNMENT

Prior to recording double exposure holograms of the disk resonant response under conditions of rotation, optical-mechanical alignment of the system has to be achieved. Initially, a point light source from a HeNe laser is directed onto the object via the same optics used with the ruby laser. The derotator is switched to manual and set to rotate

at a slow speed. If the axis of rotation of the derotator is pointed
directly at the point source, the image formed will describe a circle.
If the derotator prism axis is not collinear with the rotational axis
of the drive motor, the image formed will describe an epicycle. The
epicycle is reduced to a circle by adjusting the angular orientation of
the Abbe prism. Now, it is necessary to reduce the circle to a single
point. This will ensure that the derotator optical axis and the object
rotational axis are now collinear and aligned. This is accomplished by
adjusting the mirror system M1 in Figure 4 with the object stationary
and then a final adjustment with it spinning and phase-locked with the
derotator. A check of the alignment is made under rotating conditions
by making a double exposure hologram without any resonant excitation.
The resulting exposed hologram will yield a group of parallel bias fringes
across the face of the disk surface whose spacing is proportional to the
degree of misalignment. If the number of these bias fringes approaches
the same order of fringes formed from disk normal displacement resulting
from resonant excitation, a confusing hologram will result and the sys-
tem has to be realigned. However, if the double exposure hologram has
fewer than five bias fringes, the system degree of alignment is more than
adequate to achieve distinctly defined resonant mode shapes under rotating
conditions.

5. NUMERICAL ANALYSIS

The numerical portion of the study was based on finite element
methods and classical solutions readily available for circular plates.
Only the first five diametral modes and the coupled (2n-1s) mode were
investigated.

Leissa (Reference 7) has generated tables of eigenvalues for annu-
lar plates consisting of circular outer boundary (a) and a concentric
circular inner boundary (b) with constant thickness (T). Various com-
binations of simple boundary conditions are presented for a Poisson's
ratio of 1/3. These tables were applied to a disk which was assumed to

14

be free on the outside and clamped on the inside. The outside radius
was 5 inches and inside radius one half inch with a thickness of 1/16
inch. This simulates the disk geometry which was used in the experi-
mental set-up. Based on this configuration and Leissa's tables, the
first five nodal diameters and the coupled (2n-1s) mode were calculated
for nonrotating conditions.

The finite element computer program NASTRAN was used
to compute the natural frequencies and mode shapes for a circular annu-
lar plate under nonrotating conditions and increasing centrifugal loading
up to 10,000 rpm. The annulus of the plate was fixed against translation
and rotation with the geometry being the same as that used in the classi-
cal solutions and experimental set-up.

The type of element used was the quadrilateral plate bending
element called CQUAD2 (this is a name for a 4-sided element in the finite
element method used in NASTRAN). This element has both inplane and bend-
ing stiffness that assumes a solid homogeneous cross section. The ele-
ments used were kept as nearly square as practicable because the accuracy
tends to deteriorate as the aspect ratio of the quadrilateral increases.

The mesh composed of CQUAD2 elements was used in the eigenvalue
extraction routine of the inverse power method to determine the natural
frequencies of vibration. This is a stand-alone method in NASTRAN and
the routine finds all the eigenvalues within a domain specified by the
user.

In addition to computing natural frequencies, the version of NASTRAN
used at the Air Force Aero-Propulsion Laboratory permits contour plots
to be made of the vibration mode shapes showing out-of-plane displace-
ment in the Z-direction (normal to the plane of the plate). This plot-
ting was conducted for the modes of interest.

In this study we wanted to investigate the vibratory response of the plate under the additional influence of centrifugal loading. This was necessary to verify the results obtained experimentally using the image derotator. Because of the cost of running such an analysis on the computer, only one mode of vibration was investigated at rpms of 2,000, 4,000, 6,000, and 8,000.

Rigid format 13 of NASTRAN was used to compute the natural frequencies and mode shapes for the one case. NASTRAN performs the vibrational analysis in a two-step operation. First, it takes the value of the angular velocity input to it and creates a set of forces that act on the element centroids of the finite element model. These forces are a function of the mass of the element, their locations with respect to the axis of rotation, and the angular velocity. Using these forces, a static analysis is carried out (rigid format 1) and the resulting stresses are used to generate a centrifugal stiffness matrix. In the second step of this operation, the centrifugal stiffness matrix is added to the NAS-TRAN-generated elastic stiffness matrix and an eigenvalue analysis is carried out (rigid format 3) yielding the natural frequencies of the structure. This two-step process is carried out automatically using rigid format 13 of NASTRAN.

SECTION III

RESULTS

1.   EXPERIMENTAL RESULTS

In order to have a reference for the disk mode shapes obtained under rotating conditions, the first five diametrical modes of vibration (1n, 0s) through (5n, 0s) and second coupled mode of vibration (2n, 1s) for the steel disk fixed at its center were determined using time-averaged holography. Except when noted, the 0s portion of the mode notation shall be implied.

Figures 10 and 11 show the six resonant modes obtained statically using siren excitation and a standard off-axis holographic set-up with a 50 MW HeNe laser as described previously. Resonance was determined by monitoring the out-of-plane displacement with a capacitance probe while varying the frequency via a sweep oscillator. The outputs of each signal were fed to the horizontal, and vertical inputs to an oscilloscope, with resonance being determined by the resulting Lissajous patterns.

The brightest fringes in the figures for the holograms are the node lines which are points of zero displacement forming diametrically across the face of the disk; hence, the terminology diametral modes. The couple mode shown in Figure 11 (1052 HZ) is a combination of diametrical modes plus circumferential modes running around the periphery of the disk.

The node line orientation was governed primarily by the location of the siren relative to the disk. The point of excitement could be localized to approximately a one-inch diameter circle. At this point, the mode pattern oriented itself such that an antinode (point of maximum displacement which bisects two adjacent node lines) was generated at the siren excitation location. However, it was discovered that by

17

lowering the siren excitation power the modes assumed a preferred orientation. This was comprised of two sets of node patterns for each mode of vibration. They were essentially the inverse of each other with the nodal lines of one becoming the antinodal lines of the other; i.e., the node line which was the point of zero displacement now becomes the antinode line or point of maximum displacement. The preferred orientation is a result of the imperfection of the disk (Reference 4), which is present in all practical cases. The two-mode patterns differed in natural frequencies by an amount depending on the degree of imperfection. These modes are quite independent of each other, and their nodal patterns coincide with those of maximum and minimum frequency. The nodal diameter of one and an antinodal diameter of the other will pass through the imperfection. The frequency of the former will be greater than that of the latter.

For the steel disk in this experiment, the frequency spread ranged from 0.5 to 1.5 hertz depending on the mode being excited. This small difference is indicative of the high degree of radial symmetry present in the mass and stiffness characteristics of the disk. It can be shown that in the case of the disk with perfect radial symmetry, that each of the mode pairs will degenerate to a single mode shape and corresponding resonant frequency having random node orientation. Thus, a perfect disk would have no preferred node orientation. An imperfect disk under conditions of free vibration would have two node patterns for each mode whose frequency spread depends on the amount of unsymmetry. Under conditions of forced vibration, only one mode pattern will appear with its orientation depending on the excitation source location.

The disk was mounted to the lathe motor and its resonance response was determined under rotating conditions. Figures 12 and 13 show the results which describe the phenomena mentioned previously in the discussion. This demonstrates that for each mode of vibration two excitation frequencies will excite the same resonant mode. In other words, at a

18

specific disk rpm, the 2n mode of vibration will be excited into reso-
nance by two different excitation frequencies, one that is 2Ω greater
than the 2n natural frequency and one that is 2Ω less than the 2n natur-
al frequency. Shown are the upper and lower resonant conditions for the
1n, 2n, 3n, 4n, and 5n modes, respectively.

The plots (Figures 12 and 13) depict the frequency of an electro-
magnetic exciter required to generate a resonant disk mode versus the
disk speed. The data points represent a maximum response indication
from a capacitance probe placed near the back face of the disk (see
Figure 4, "Vibration Pickup"). The curve joining each set of data points
is a second order least squares fit. As discussed, the upper curve for
each mode of vibration is a plot of $p_n + n\,\Omega$. As the disk speed decreases
to zero, the upper and lower branches of the excitation frequency con-
verge to the corresponding resonant frequency for the stationary disk.
The dashed lines in Figure 12 represent extrapolated data and show the
2n and 3n modes crossing the abscissa at 5600 and 7600 rpm, respectively.
At these points, a resonant mode can be excited by a static force. This
would be a particularly dangerous region of operation for a turbine engine
disk since a circumferential variation in the existing pressure field could
generate a resonant response. These two resonant points are often re-
ferred to in a "Campbell Diagram" used by turbine engine designers. The
diagram is established by bisecting the upper and lower resonant lines
shown in Figures 12 and 13. This determines the natural frequencies for
each disk mode. Then engine order lines are plotted which are equal to
the number of excitations per disk revolution (1E, 2E, 3E, etc.). Now,
the 2E engine order line will cross the 2n mode natural frequency at 5600
rpm and have a value of 5600 x 2E/60 = 187 Hz. Likewise, the 3E engine
order line will cross the 3n mode natural frequency at 7600 rpm and have
a value of 7600 x 3E/60 = 380 Hz. The Campbell Diagram is then used by
the designer to identify possible resonant points which should be avoided
during engine operation.

Figures 14 and 15 show the same disk resonant mode shapes that were obtained under stationary conditions (Figures 10 and 11) obtained using image derotated holographic interferometry at specified disk speeds. The mode shapes shown in the figures are double exposure holograms made using the pulsed ruby laser with a pulse separation of 20 μs. It is seen that the fringe contrast is quite good and almost entirely proportional to disk out-of-plane displacement with very little distortion introduced from bias fringes caused by opto-mechanical misalignment. Each mode shape in Figures 14 and 15 corresponds to some point on one of the excitation frequency - disk speed curves in Figures 12 and 13. For example, the 4n mode shape in Figure 15 was excited at 724 Hz when the disk was rotating at 2620 rpm. This point lies on the upper branch of the 4n curve in Figure 13. The actual natural frequency for the mode at this rpm would thus be:

$$P4 = F_{E4} - n\,\Omega = 724 - (4)(2620)/60 = 549 \text{ Hz}$$

This is an increase of 12 Hz over the 4n natural frequency for the nonrotating disk. Figure 16 shows the same 4n mode shape obtained while the disk was running at 7920 rpm. The very minor contribution of bias fringes, i.e., the two fringes running approximately across the diameter of the disk, demonstrates the stability of the system even at speeds near the upper design limit of the derotator (10,000 rpm).

Figures 14, 15, and 16 show modes of vibration that are fairly pure in their nature, i.e., mode shapes characteristic of classical disk vibration theory. Disk mode shapes were also recorded that were apparently combinations of more than one resonant mode shape. This type of response would manifest itself as the actual resonant mode shape being excited and distorted typically by the 1n mode shape. This type of response was thought to be caused by an additional disk excitation force resulting from rotor dynamic imbalance of the disk shaft. This phenomenon was subsequently verified by carrying out a power spectral

20

density analysis of the vibration transducer signal with and without disk excitation. The excitation component due to shaft imbalance was not found to present a problem provided that the amplitude of the electromagnetic excitation was an order of magnitude larger than the force from the dynamic shaft imbalance. There was no added complication in increasing the electromagnetic force amplitude since the laser pulse separation could be decreased proportionally in order to avoid "wash out" of the holographic fringes from too large a disk displacement.

2. FINITE ELEMENT ANALYSIS AND THEORETICAL CORRELATIONS

The finite element results were based on a mesh shown in Figure 17 which was generated to simulate the steel disk used in the experimental work. It was internally clamped along an inner radius (b = 1/2 inch) and unconstrained along the outer radius (a = 5 inches). Care was taken to maintain a length to width ratio of approximately one for the element blocks to ensure accuracy.

The finite element results are shown in Figures 18 and 19 for the modes of vibration which were determined experimentally under static conditions. The contour numbers in the figures correspond to values of displacement in the Z-direction (out of the paper) such that the integers 1, 2, 3, 4, 5, 6, 7, 8, 9, 10, and 11 refer to the Z-displacement values -1., -0.8, -0.6, -0.4, -0.2, 0, 1.3, 0.4, 0.6, 0.8, and 1., respectively. Note that contour number 6 corresponds to a Z-displacement of zero and hence, defines the vibration nodal lines for each mode shape. For the purpose of this work, the nodal line 6 was further darkened by hand to enhance its visibility. The contour plots shown serve to graphically display the deformation characteristics of each mode of vibration. Note that all the modes exhibit either diametral and/or circumferential symmetry about the surface of the disk which is typical of classical plate vibration response.

Leissa's tables based on classical solutions for circular plates were used to establish the nondimensional frequency parameter λ^2 where

$$\lambda^2 = \omega a^2 (\rho/D)^{1/2}$$

$$D = ET^3/12 \ (1-\nu^2)$$

(4)

Using the tabulated values of λ^2, we solved Equation 4 for ω in radians/ sec for the same frequencies determined experimentally. For this case, the following properties (same as the steel disk) were used: radius, a = 5.0 inches, thickness, T = 0.0625 inches, Poisson's ratio, ν = 0.3, Young's modulus, E = 3.05 x 10^7 psi, mass/area, ρ = 1.768 x 10^{-2} lbm/in^2. The parameter D is known as the flexural rigidity and is constant for a given configuration. Table 1 shows the correlation between the experimental results, finite element, and frequencies determined using Leissa's tables (Reference 7). There was a large discrepancy between the numerical techniques and the experimental results. The difference was judged to be caused primarily by the boundary conditions imposed on the numerical technique versus the steel hub configuration used in the experimental work. An experiment was conducted (see Appendix B) using a different configuration for clamping the disk which was considered to be more representative of the numerical boundary constraints. The disk was tested experimentally and results compared to analytical calculations of frequencies. Correlation, in most cases, was less than a 2% difference, leading to the conclusion that the integral hub for the steel disk does not constrain the inner radius as was originally thought. However, the purpose of the research was to prove the merits of the image derotator, so that discrepancies between experimental and analytical techniques are of little concern.

The finite element program was further used to provide an analytical check on the effect of centrifugal loading on the resonant frequencies of the disk. Figure 20 shows a plot of the disk mode (3n, 0s) resonant

frequency as a function of rpm for both the finite element and experi-
mental results. The experimental resonant frequencies were approximately
4% below those computed from the finite element model. This was felt to
be sufficiently accurate considering the large effects the hub can have
on the boundary conditions as previously determined for the nonrotating
calculations.

SECTION IV

CONCLUSIONS

Image derotation techniques in conjunction with double-pulsed laser technology has opened new avenues for research in addressing the area of dynamic structural response of rotating structures. The emphasis of the research was to demonstrate the graphic results which can be obtained by applying image derotated holographic interferometry to a simple disk under conditions of rotation. With this in mind, it should be noted that the characteristic movement of the mode shapes relative to the disk requires a much more detailed analysis than was possible within the scope of this present work. The shapes recorded under rotating conditions such as Figures 14 and 15 do not provide information as to the relative movement of the mode in relation to the disk. One has to determine whether the mode is fixed to the disk and hence rotating with it, or is stationary in initial space with the disk rotating through it, or is a movement of some combination in between. It can be easily shown that the derotator and pulsed laser combinations permit disk mode shapes to be recorded under any of these conditions.

Attempts were made to determine the relative movement of the mode shapes by consecutively recording a series of interferograms while keeping the disk rpm and vibration excitation amplitude constant and observing the location of the node lines relative to an arrowhead drawn on the disk. The results were inconclusive because of difficulty encountered in keeping the rpm constant over a period of time. This drifting caused phase shifts in the vibratory response of the disk and the resulting holograms showed a random orientation of the mode patterns and thus they did not seem fixed to the disk or in inertial space. Tobias (Reference 4) carried out a detailed study of the vibrational characteristics of an imperfect rotating disk and analytically demonstrated that the relative movement of the mode shapes was directly related to the phase shifts as the rotating disk passes through a resonant point. It is felt that if the same phase could be obtained over a given period of time, the movement of the node lines could be determined.

24

The above questions still need answers in order to completely understand the resonant response of rotating structures to provide increased assurance as to their structural integrity. The phenomena of vibrational response of a rotating disk is complex in itself; the addition of blades to the structure further complicates the problem. This is demonstrated in Figure 21, which shows a bladed disk assembly vibrating in one of its many resonant modes under nonrotating conditions using time-averaged holography. It demonstrates the complex mode shapes which can be obtained.

Through the advent of image derotated holographic interferometry, the above questions will be addressed in future research and the complex vibratory behavior exemplified by Figure 21 shall be studied.

APPENDIX A

BURST SPEED CALCULATION

In the interest of safety, it was necessary to calculate the burst speed of the steel disk which was used for the rotational aspects of the experimental investigation. Rotational speeds approaching 10,000 rpm were expected and subsequently used as the design limit.

According to Roark (Reference 8), formulas for calculating burst speeds should be based on an average stress instead of a maximum stress. This is because the formulas for determining the maximum stress pre-supposes elastic conditions and does not account for plastic yielding prior to failure. This yielding tends to equalize the stress intensity along a radial line.

Roark's formula for calculating the average stress, σ_a is:

$$\sigma_a = \frac{0.000863\delta\omega^2 (a^3 - b^3)}{a - b}$$

where δ is the density, ω is the angular velocity, a and b, respectively, are the outside and inside radii. Experiments have shown that for the worst cases, annular disks have failed when a reaches 61.5% of the ulti-mate strength. Based on this criteria, a value of 36,900 psi was assumed for the design stress and the above equation solved for ω. This was converted to rpm or burst speed and found to be 23,031 rpm. This value compared to the design limit of 10,000 rpm for the derotator, was suf-ficient to provide a margin of safety.

APPENDIX B

HUB EFFECTS ON FREQUENCIES

The discrepancies found between the numerical and experimental results in determining modes of vibrations were largely attributed to the integral hub machined for the steel disk. This was verified by investigating another means of clamping a circular disk to a shaft and again comparing the experimental frequencies with classical numerical solutions.

A 0.0625-inch-thick aluminum disk, 10 inches in diameter, with a 0.25-inch diameter center hole, was manufactured without an integral hub as described previously for the steel disk. A new clamping fixture, as shown in Figure 21, was made from aluminum and designed to simulate an annular disk consisting of a free circular outer boundary and a clamped circular inner boundary with an inner-to-outer radius ratio of 0.1. It was felt that this design would be more representative than that of the integral hub for matching the boundary constraints used in the numerical calculations, i.e., zero slope and zero deflection at the inner radius.

The aluminum disk was mounted with new clamps to an isolation table and excited into resonance, using a siren driven by a sweep oscillator. Real-time holography was used to determine the first nine modes of vibrations which included circumferential modes. Table 2 is a listing of the experimental results compared to frequencies determined analytically using Leissa's tabulated values of eigenvalues along with the flexural rigidity constant determined for the aluminum disk.

Excellent correlation was obtained between the experimental and numerical techniques for established modal frequencies. In most cases, the difference was less than 2%. The larger variation found for the (1n, 0s) mode can be attributed to the fact that this mode exerts a couple on the shaft transverse to its length with the inner radius not being rigidly constrained as in the numerical solutions. The other modes are symmetrical and thus balanced in their reactions on the shaft resulting in zero slope and zero deflections around the inner circumference of clamping as in the numerical solution.

It was concluded that the integral hub manufactured with the steel disk has a large effect on the stiffening characteristics and boundary conditions of the system which, in turn, affects the experimental results. However, the purpose of the research was to prove the merits of image de-rotator in studying the vibrational characteristics of a rotating structure. More importantly, one should note that, even the simplest geometry of a steel disk with an integral hub is very difficult to model numerically and results can often be misleading. It is imperative that experimental techniques be continuously developed for the investigations of structures, especially more complex configurations such as bladed disk assemblies. Numerical methods have to have input from experimental methods to ensure their validity.

APPENDIX C

EQUIPMENT

The following is a list of test equipment used throughout the experimental aspects of the study:

1. Double Pulse Ruby Laser
   Apollo Lasers, Model 22, S/N 283
   PW 20n Sec, 2.5J Pulse

2. He-Ne Laser
   Spectra Physics Model 125A, S/N 3109-875
   CW; 50MW Power

3. Storage Oscilloscope
   Tektronix Inc., Model 7633, S/N JH Ø 177

4. Oscilloscope
   Tektronix Inc., Type 531, S/N 1051

5. Universal Counter
   Hewlett Packard, Model 5325B, S/N 5090J

6. Sweep Oscillator
   Spectral Dynamics Corp., Model SD104A-5, S/N 1477

7. Tracking Filter (Dynamic Analyzer)
   Spectral Dynamics Corp., Model SD101B, S/N 645

8. Charge/Voltage Amplifier
   Unholtz-Dickie, Model D22, S/N PJ6501

9. Tool Post Grinder
   Dumore, Cat. No. 57-011, S/N 8476-01914
   RPM 10,500 HP 3/4

10. Power Amplifier
    Bell Sound Division, Model Mark 40, S/N JC8056

11. Amplitude Servo/Monitor
    Spectral Dynamics Corp., Model SD 105C, S/N 5969J

12. 35MM Film Transport
    Jodon Engineering Associates

13. Siren
    University Sound, Model 1D-60T
    60 Watt, Multi-Impedance

14. Image Derotator/Phase Lock Control Unit
    Per Contract F33615-75-C-2013

15. Displacement Pickup - Capacitance Transducer
    Brüel & Kjaer, OOO4MM, 108pf, S/N PJ6036

16. Electro Magnetic Exciter
    Electro, Model 3015 HTB

17. Miscellaneous Mirrors, Plate Holders, Beam Splitters,
    and Beam Expanders:
    Jodon Engineering Associates
    Gaertner Scientific Corp.
    Newport Research Corp.

REFERENCES

1.   W. E. Campbell, "The Protection of Steam-Turbine Disc Wheels from Axial Vibration," ASME Spring Meeting, Cleveland (May 1924).

2.   P. Waddell, et al., "Pocket Cell Stroboscopic Holography for the Vibration Analysis of Objects," International Symposium on the Applications of Holography (Paper 6-6), Besancon, France, (July 1970).

3.   K. A. Stetson and J. N. Elkins, Optical System for Dynamic Analysis of Rotating Structures, AFAPL-TR-77-51 Air Force Aero-Propulsion Laboratory Contract F33615-75-C-2013 (Oct 1977).

4.   S. A. Tobias and R. N. Arnold, "The Influence of Dynamical Imperfection of the Vibration of Rotating Disks"; the Institution of Mechanical Engineers, Proceedings, 171, 669-670 (1957).

5.   J. C. MacBain, "Vibratory Behavior of Twisted Cantilevered Plates", Journal of Aircraft, Vol., 12, No. 4, pp. 343-349 (Apr 1975).

6.   P. Waddell, "Strain Pattern Examination", Engineering and Material Design, 17(3) (1973).

7.   A. W. Leissa, Vibration of Plates, NASA SP-160 (1969).

8.   J. S. Roark and W. C. Young, Formulas for Stress and Strain, 5th Edition, McGraw-Hill (1975).

TABLE 1

EXPERIMENTAL - ANALYTICAL CORRELATION (STEEL DISK)

MODE		EIGENVALUE λ^2			FREQUENCY HZ		
		Finite Element	Leissa	Experimental	Finite Element	Leissa	Experimental
1n	0s	3.7	3.1-3.5	4.2	91	75-86	103
2n	0s	5.7	5.5-5.6	5.0	140	135-136	123
3n	0s	12.3	12.4	11.8	303	305	289
4n	0s	21.8	21.6	21.9	535	530	537
5n	0s	34.1	33.1	34.6	836	813	849
2n	1s	37.3	37.0	42.8	915	909	1052

* From NASA SP-160 "Vibration of Plates" Tables 2.5, 2.29, and 2.30

Table I - Experimental - Analytical Correlation (Steel Disk)

TABLE 2

EXPERIMENTAL ANALYTICAL CORRELATION (ALUMINUM DISK)

MODE		EIGENVALUE λ^2		FREQUENCY HZ	
		Leissa *	Experi-mental	Leissa	Experi-mental
1n	0s	3.1-3.5	3.3	75-85	81
0n	0s	4.2	4.2	102	102
2n	0s	5.5-5.6	5.6	134-136	137
3n	0s	12.4	12.6	301	306
4n	0s	21.6	21.9	525	533
0n	1s	25.3	25.1	615	609
1n	1s	27.3	27.5	663	669
5n	0s	33.1	33.6	804	816
2n	1s	37.0	37.3	899	906

* From NASA SP-160 "Vibration of Plates", Tables 2.5, 2.29 and 2.30

Table II - Experimental Analytical Correlation
(Aluminum Disk)

34
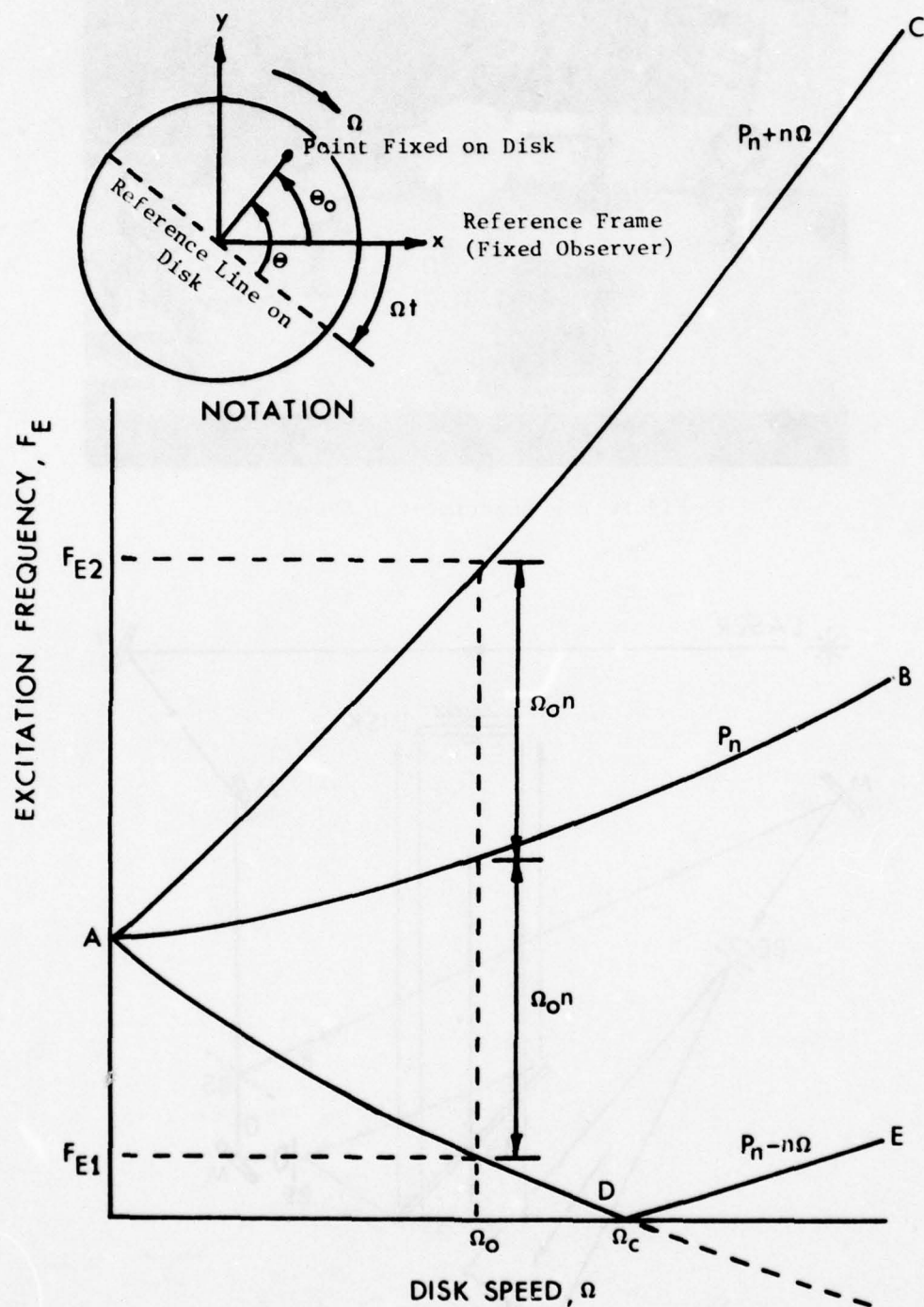
Figure 1. Frequency Speed Diagram
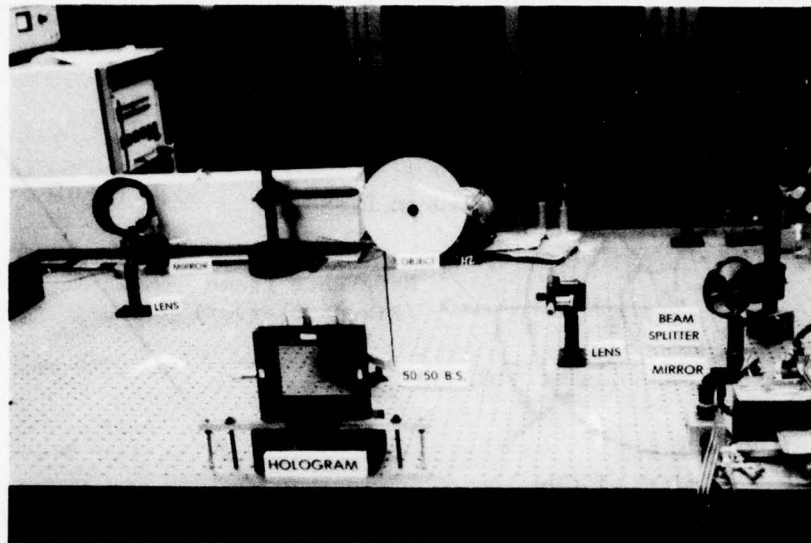
Figure 2 - Experimental Set-Up
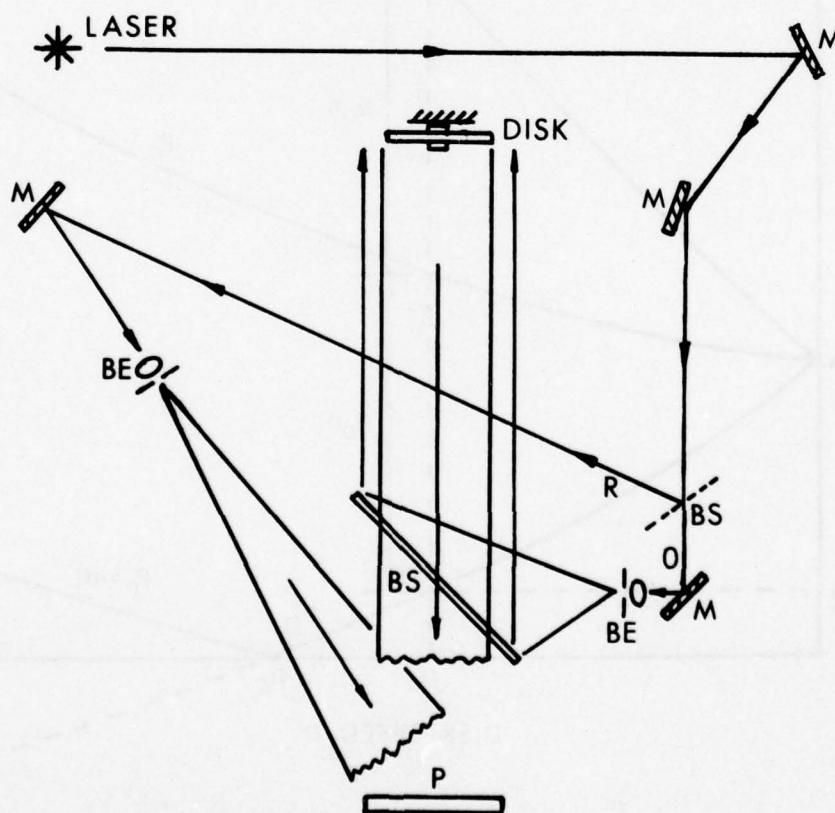
Figure 3 - Schematic of Set-Up

36
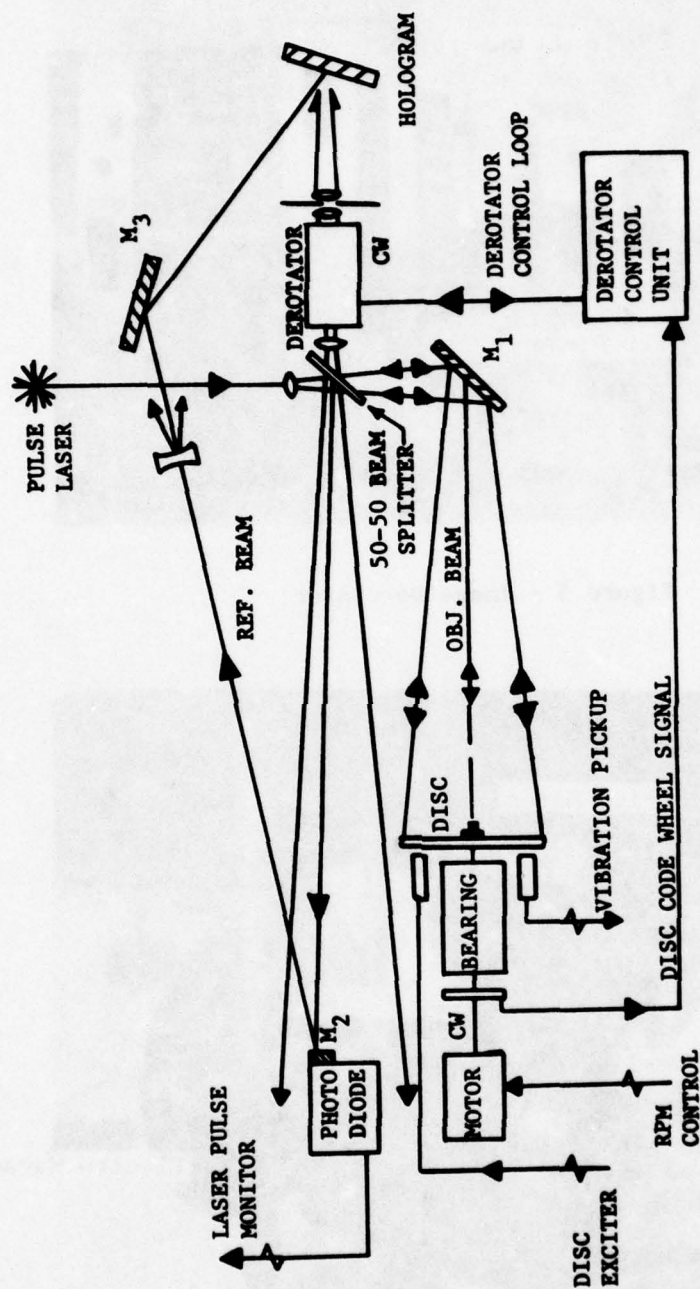
Figure 4. Experimental Set-Up for Image Derotated Holographic Interferometry
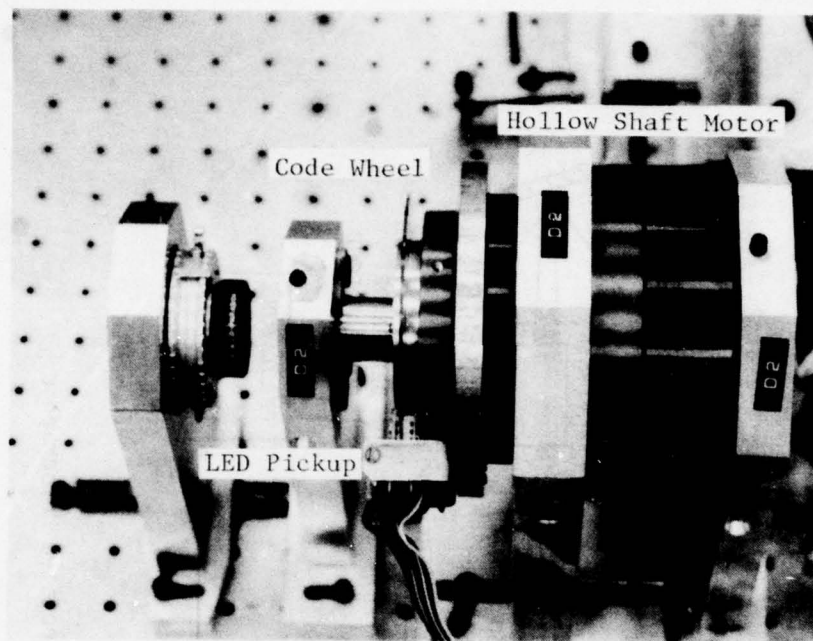
Figure 5 - Image Derotator
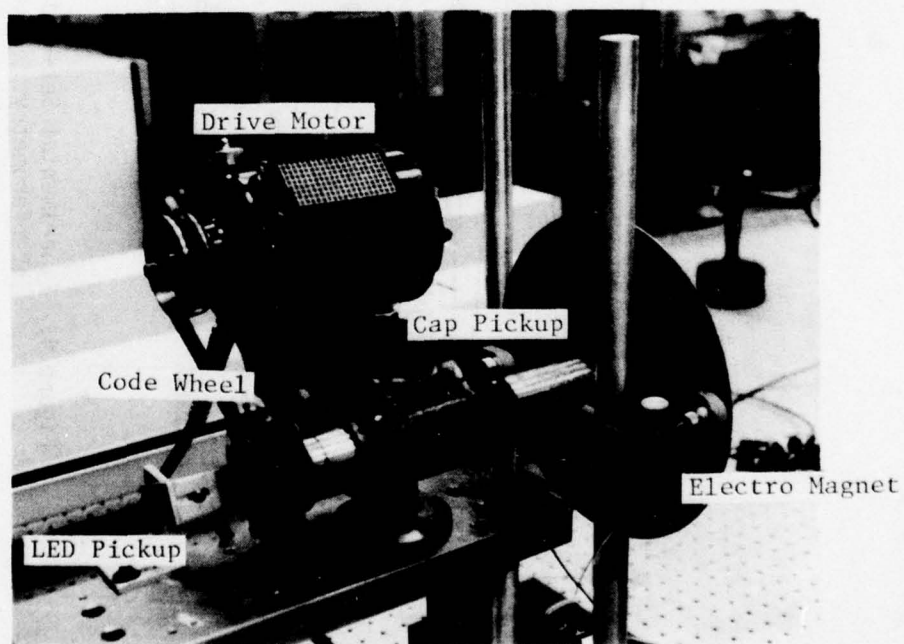
Figure 6 - Lathe Motor & Disk

38
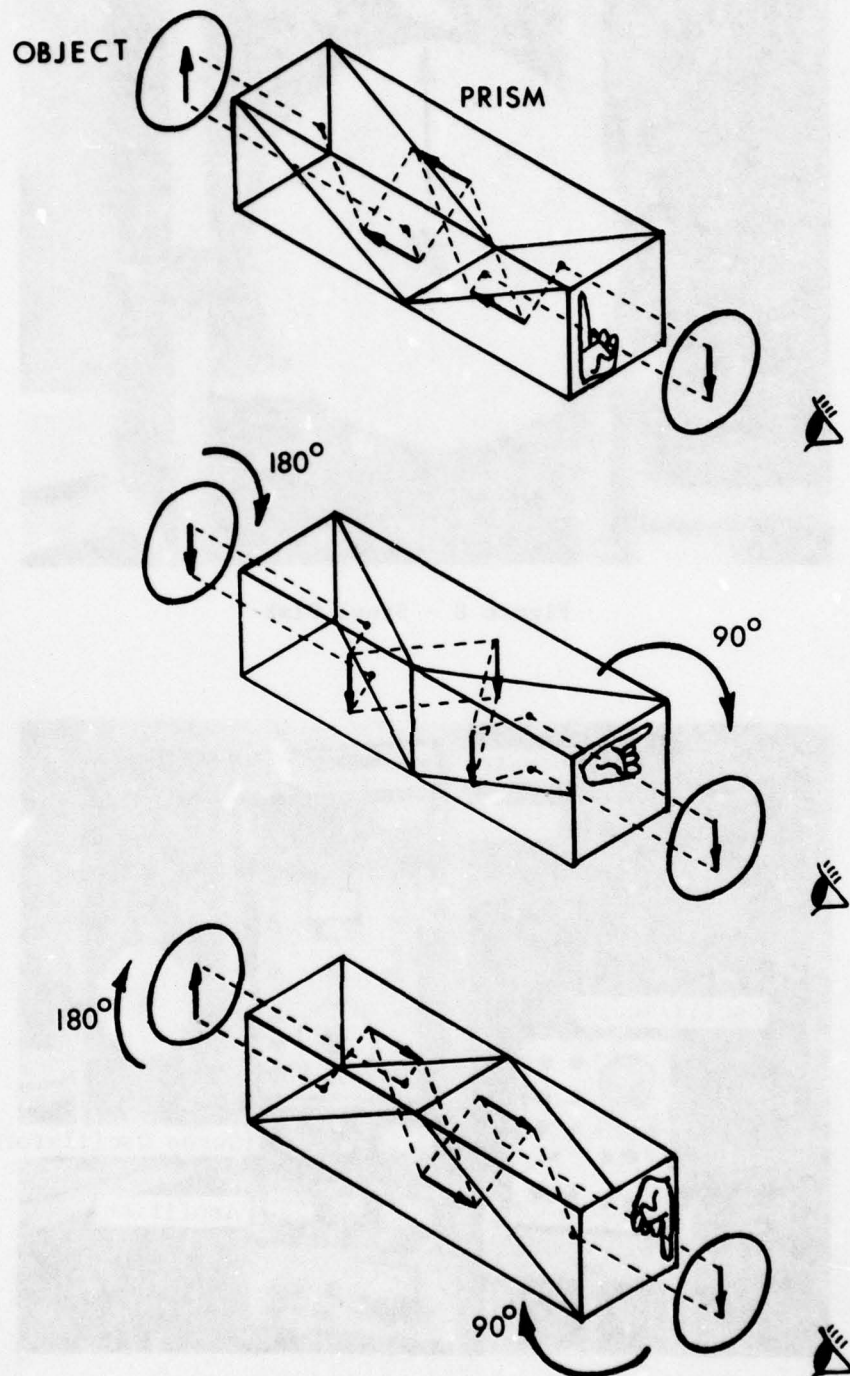
Figure 7. Folded Abbe Inverting Prism
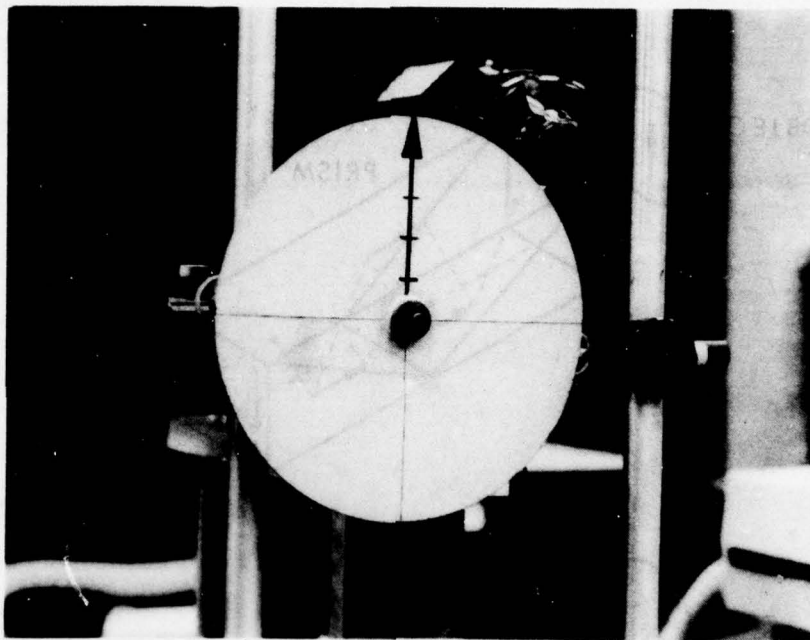
Figure 8 - Steel Disk
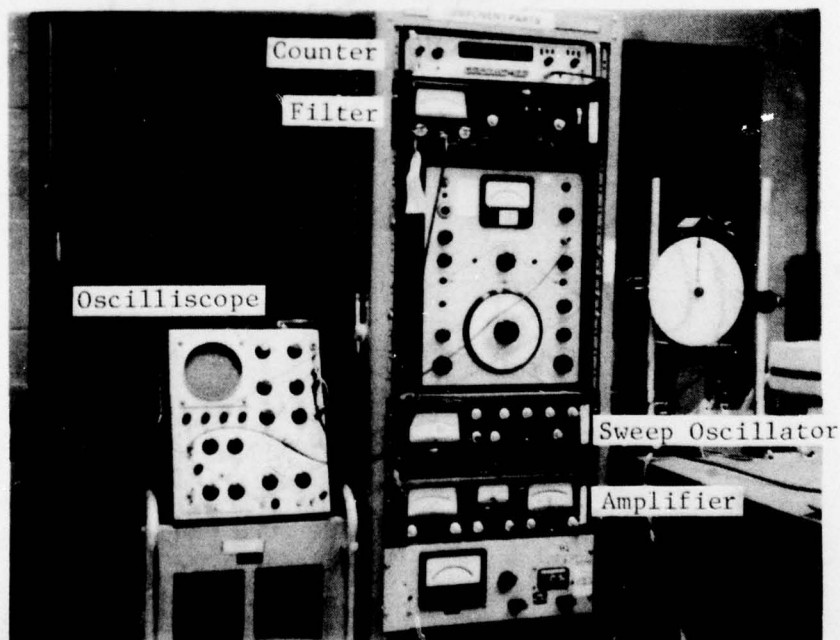
Figure 9 - Vibration Instrumentation

40
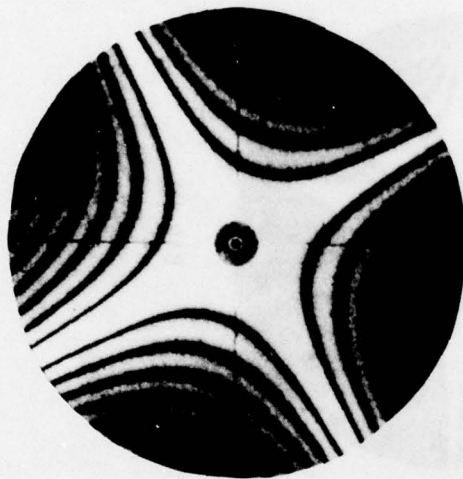
289 HZ

123 HZ

103 HZ

Figure 10 – Resonant Mode Shapes 1n, 2n, 3n for the Stationary Disk

41
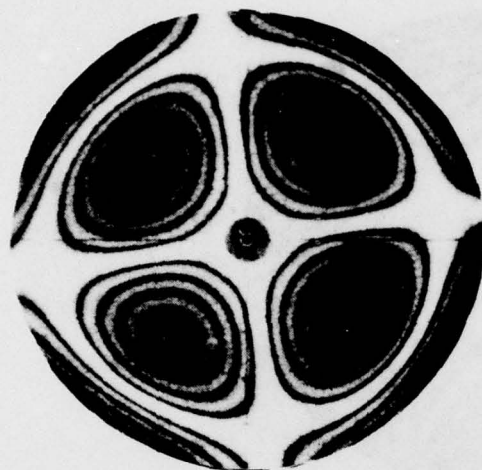
1052 HZ
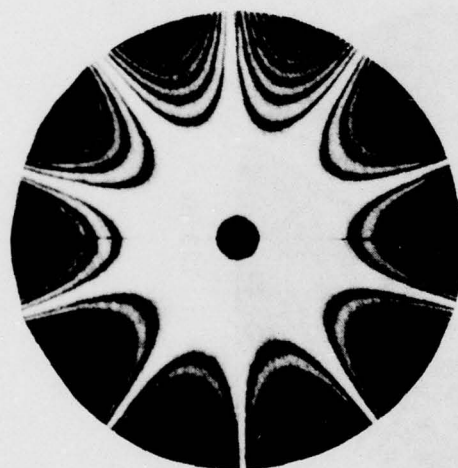
849 HZ
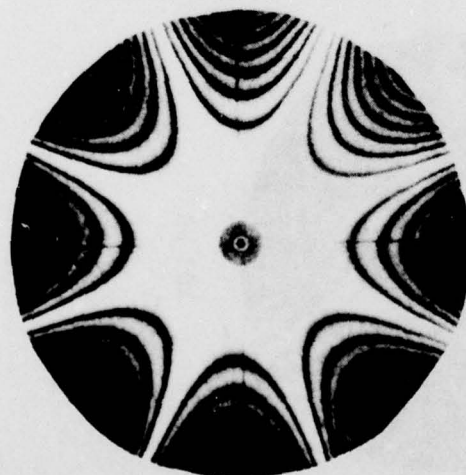
537 HZ

Figure 11 - Resonant Mode Shapes 4n, 5n, and (2n, 1s) for Stationary Disk

42
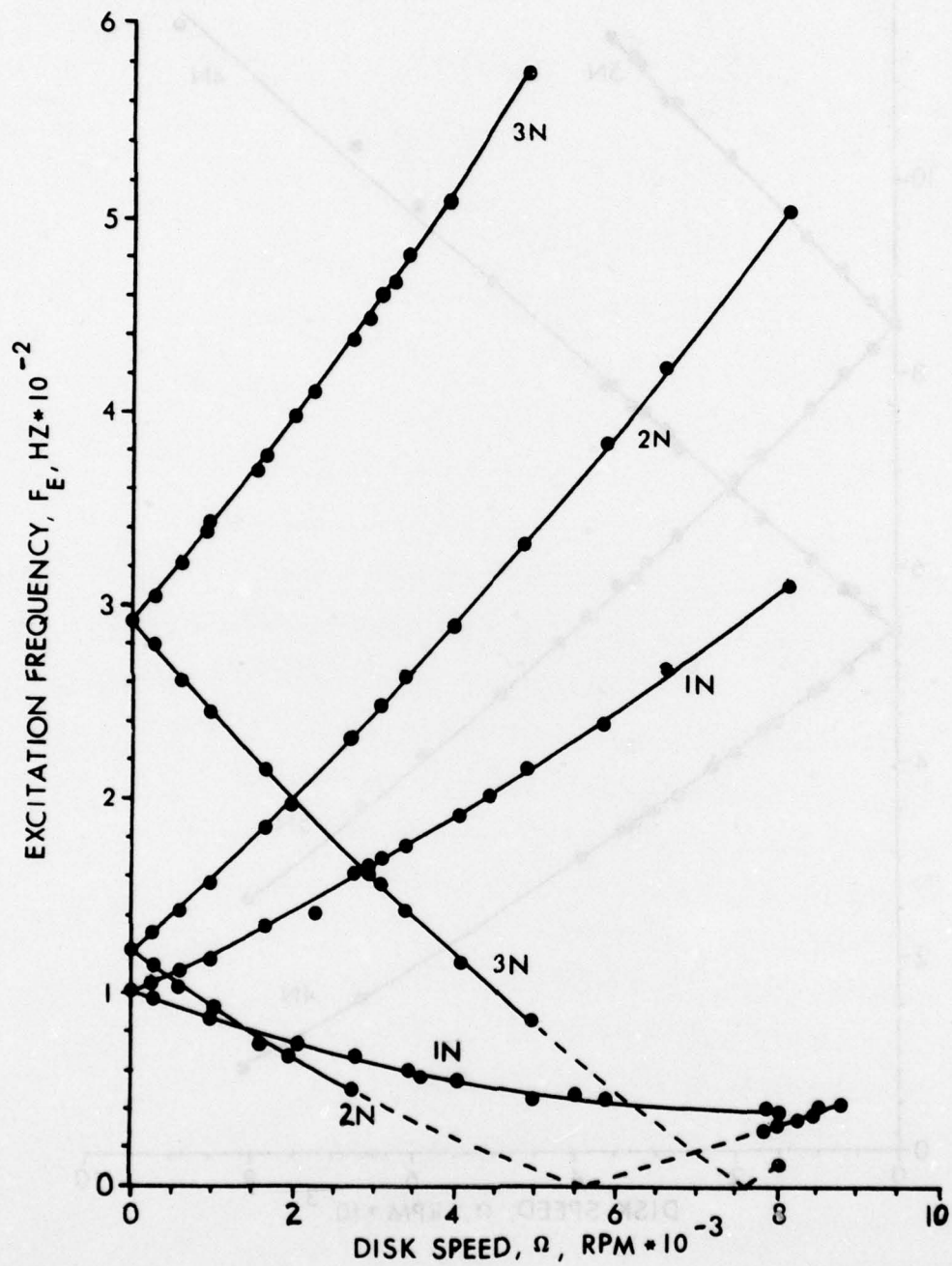
Figure 12. Resonant Excitation Frequency as a Function of Disk Speed, Modes 1n, 2n, and 3n

43
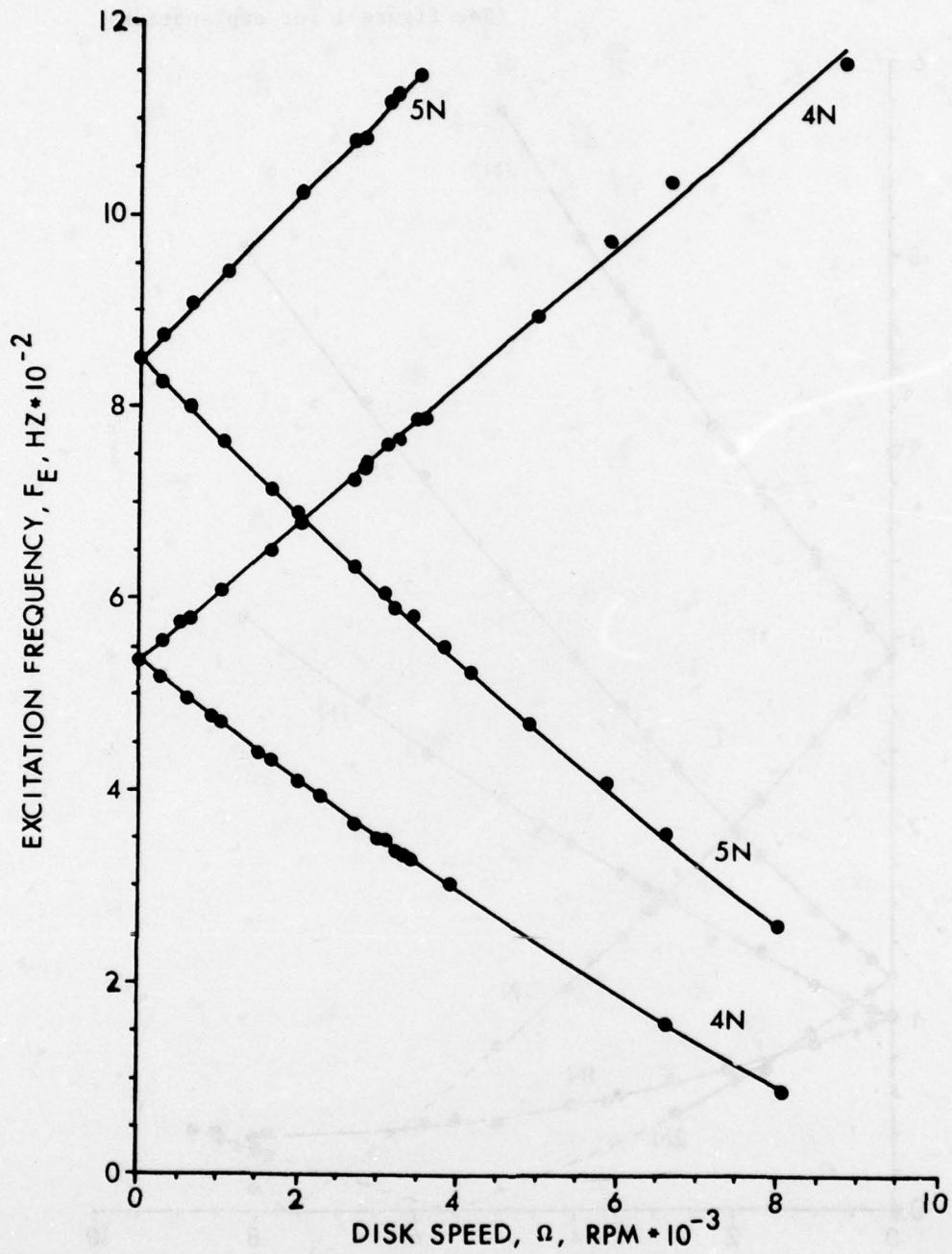
Figure 13.   Resonant Excitation Frequency as a Function of Disk Speed,
             Mode 4n and 5n
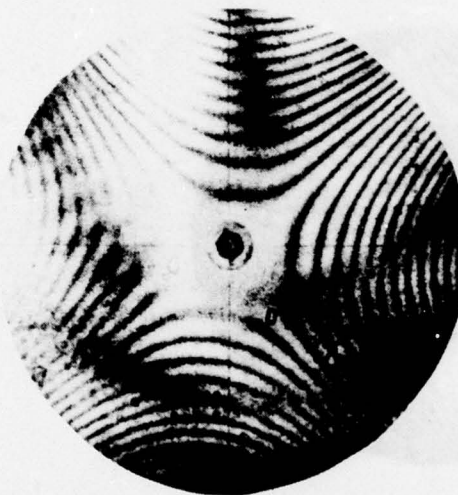
399 HZ
2020 RPM

51 HZ
2740 RPM
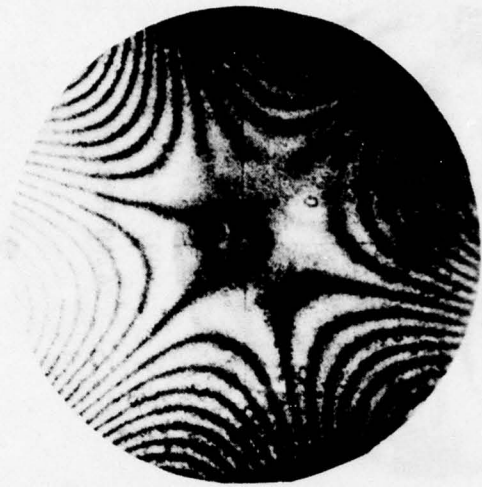
202 HZ
4440 RPM

Figure 14 - Double Exposure Holograms of Disk Modes 1n, 2n, and 3n at Specified Excitation Frequency and Disk Speed

45
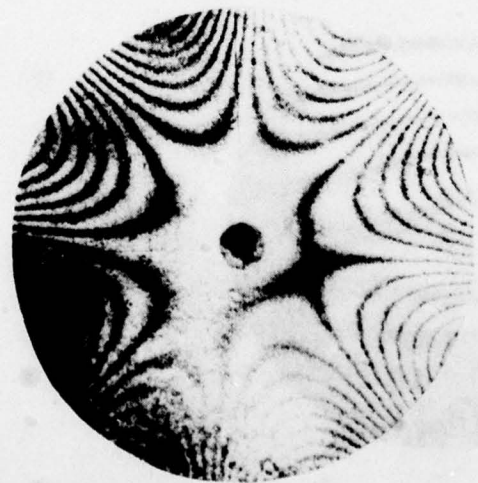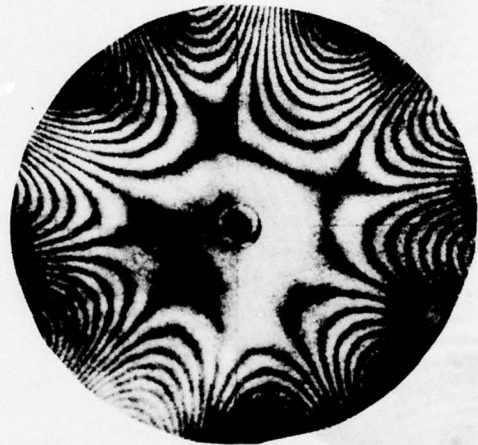
937 HZ
4140 RPM

1193 HZ
3910 RPM

724 HZ
2620 RPM

Figure 15 – Double Exposure Holograms of Disk Modes 4n, 5n, and (2n, 1s) at Specified Excitation Frequency and Disk Speed

46
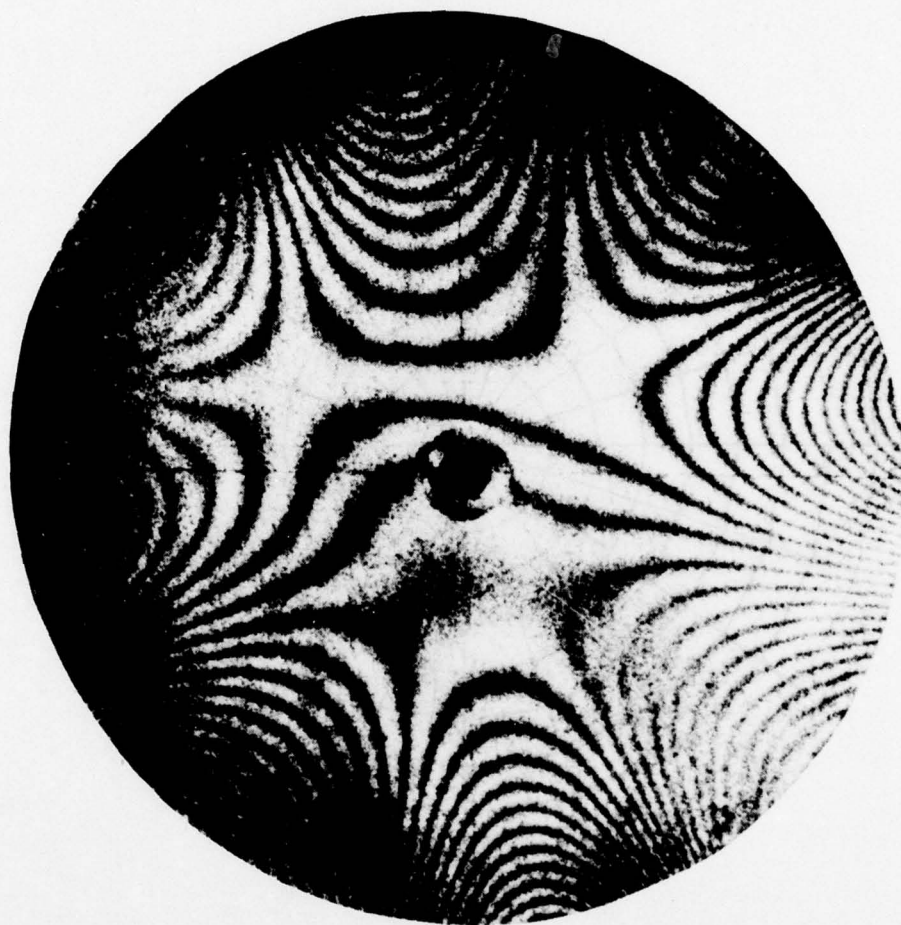
1155 HZ/7920 RPM

Figure 16 - Double Exposure Hologram of
4n Disk Mode at High RPM

47
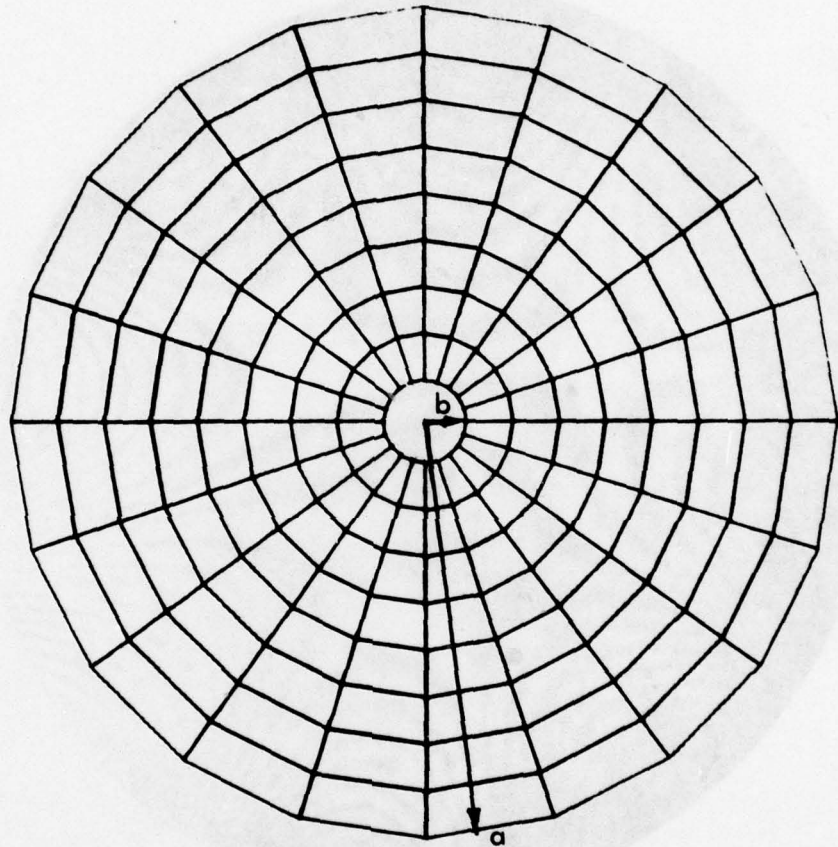
Figure 17.   Finite Element Model
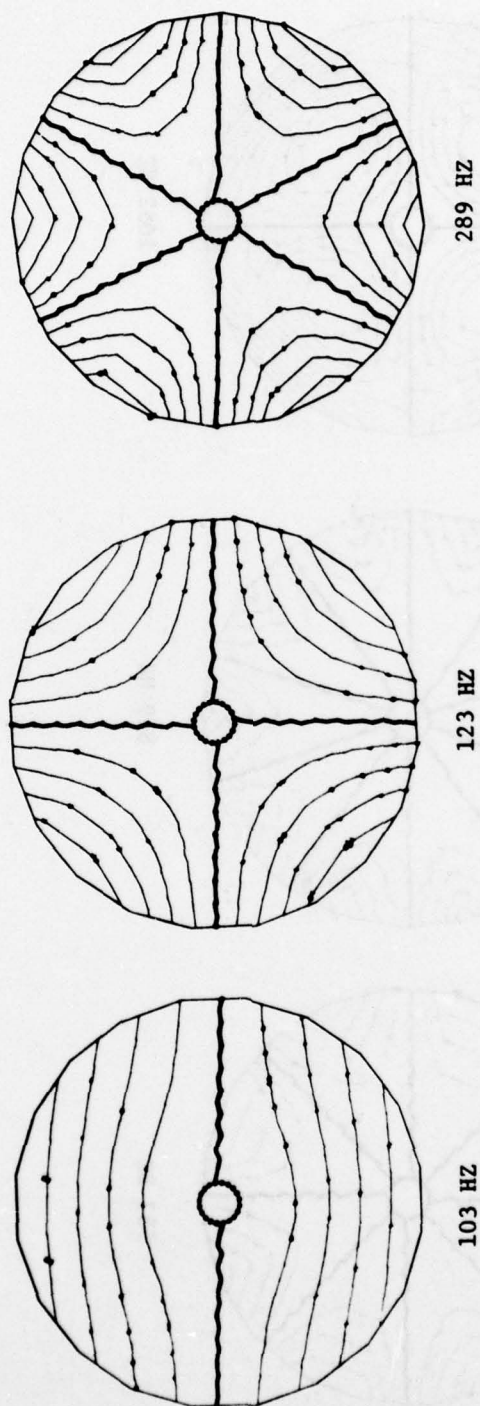
Figure 18. Finite Element Resonant Mode Shapes 1n, 2n, and 3n
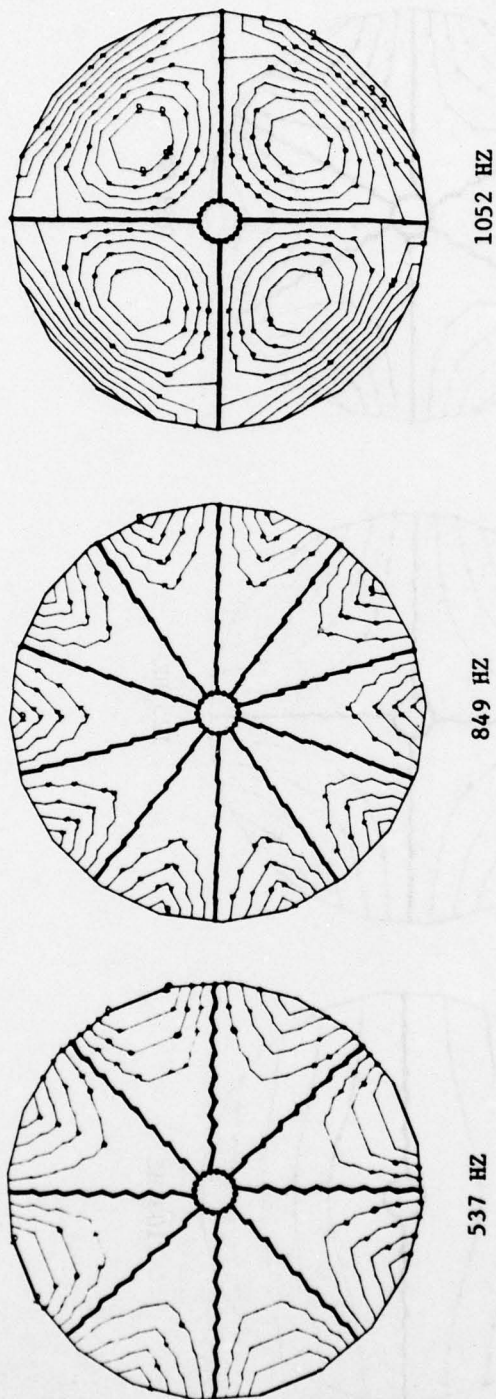
Figure 19. Finite Element Resonant Mode Shapes 4n, 5n, and (2n, 1s)

1052 HZ

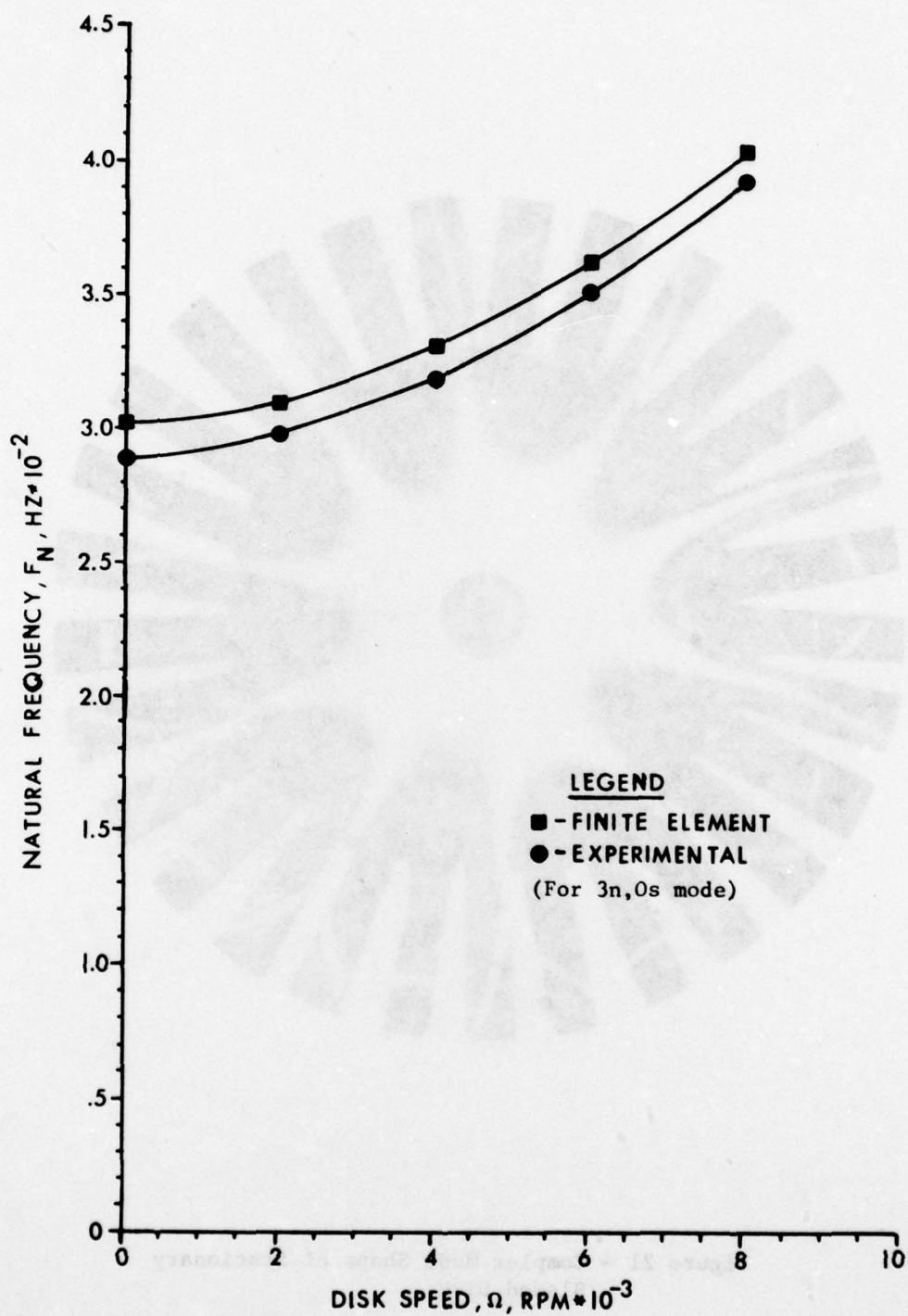849 HZ

537 HZ

Figure 20.   Disk Natural Frequency as a Function of Speed

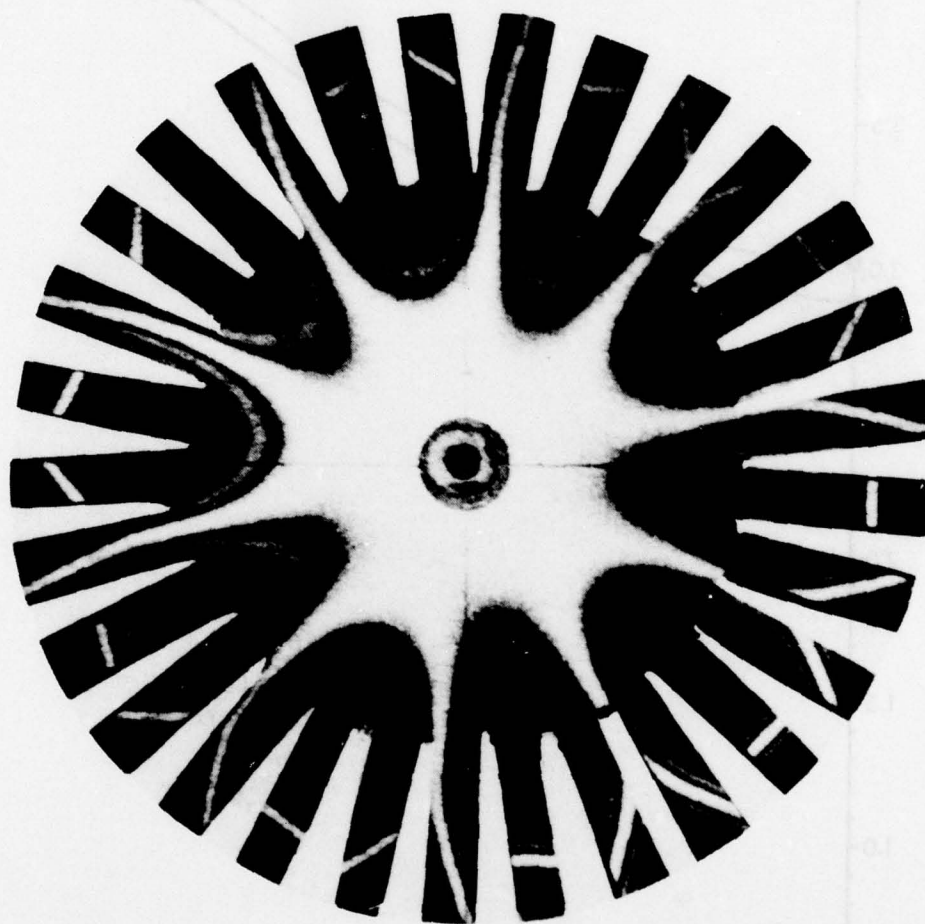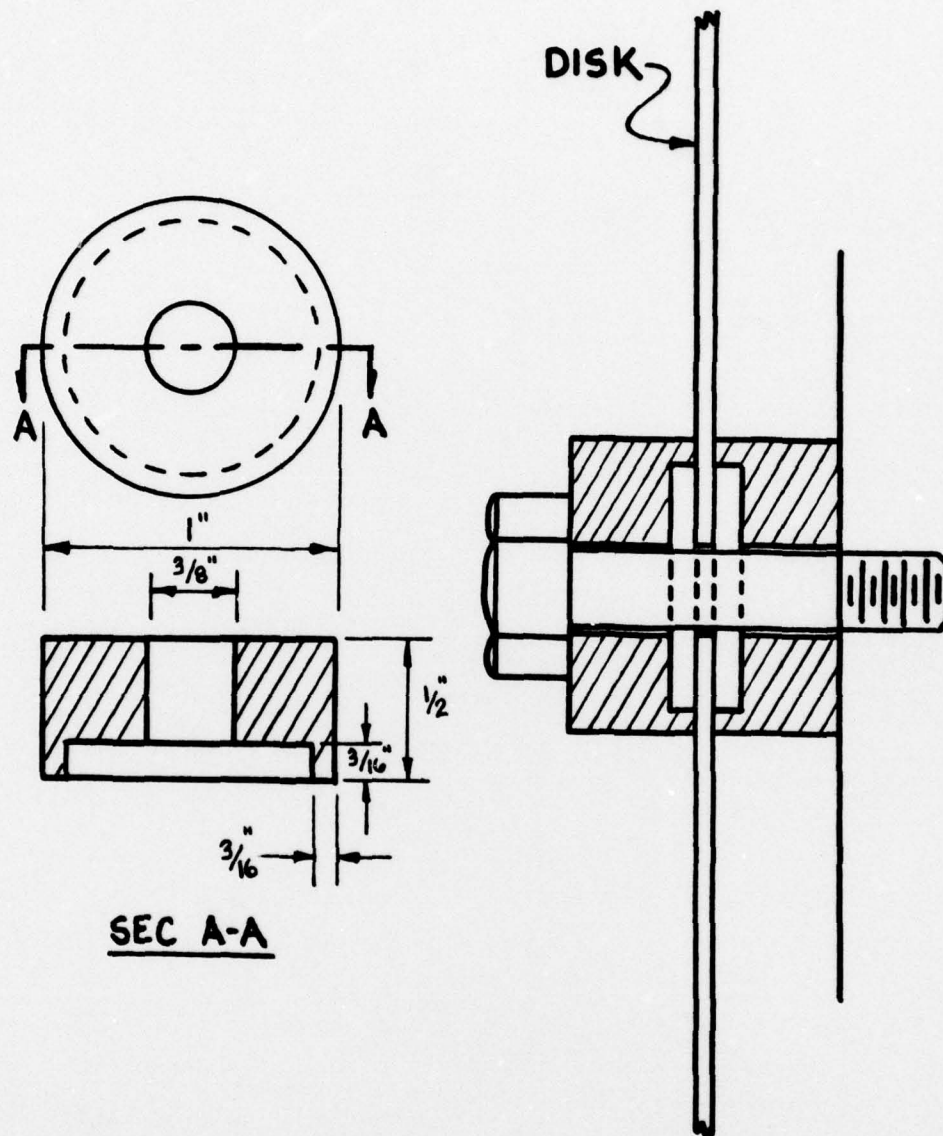Figure 21 - Complex Mode Shape of Stationary
Bladed Disk

SEC A-A

Figure 22. Clamping Fixture